

Isolation of Circulating Biomarkers for Liquid Biopsy using Immunoaffinity-Based Stimuli-Responsive Hybrid Hydrogel Beads

Yoon-Tae Kang⁺,^[a, b] Young Jun Kim⁺,^[c] Brittany Rupp,^[a, b] Emma Purcell,^[a, b] Thomas Hadlock,^[a, b] Nithya Ramnath,^[d] and Sunitha Nagrath^{*[a, b]}

This work presents chemically stable and biodegradable hydrogel beads for the isolation of circulating tumor cells (CTCs) and circulating exosomes in liquid biopsy. The liquid biopsy hydrogel beads (^{LB}beads) consisting of alginate and poly(vinyl alcohol) hydrogels show both chemical stability and stimuli-degradable characteristics. Unlike single-component hydrogels, this hybrid form is not easily degraded by buffers or cell culture media while its degradable characteristic remains; thus, it is useful in bio-applications requiring multi-step processes with various reagents and lengthy incubation periods. We applied our platform to clinical samples for isolating two promising

circulating biomarkers for a liquid biopsy, CTCs and exosomes, by conjugating the hydrogel surface with anti-EpCAM and anti-CD63 antibodies, respectively, thus achieving 37.4 CTCs and comparable amount of exosome recovery per 1 milliliter of blood. The results show easy device-free isolation and retrieval of CTCs and exosomes, with recovered circulating biomarkers successfully analyzed by western blot analysis and fluorescence microscopy. We believe that this simple and versatile platform enables us to isolate prominent circulating biomarkers for clinical use in cancer diagnosis.

Introduction

In recent years, liquid biopsy has emerged as an important technological breakthrough in medical sciences and engineering^[1-3] with considerable potential for early detection,^[4-5] diagnosis,^[6-7] prognosis,^[8-9] therapeutic outcome prediction,^[10-11] and evaluation of recurrence or disease progression.^[8-12] Unlike a conventional biopsy, which requires invasive extraction of small tissue samples through costly and stressful surgical procedures, this alternative biopsy method examines non-solid biological samples, such as blood and urine. This minimally invasive examination allows for more frequent monitoring of patients at reasonable costs, with less pain and risk involved.^[3,13] Therefore, it is expected that the socioeconomic burden of disease can be substantially lowered through this game-changing strategy.^[14] For these reasons, many researchers have been developing isolation and detection techniques for disease-related circulating biomarkers from

biological fluids. In the case of cancer research, circulating tumor cells (CTCs), circulating extracellular vesicles (e.g. exosomes) and circulating tumor nucleic acids (ctNA) are often studied.^[15-17]

Notwithstanding the recent advances and investment boom in genome-based approaches targeting ctNA, significant effort is still needed to find a correlation between cellular level- and molecular level studies.^[18-19] Specifically in the cancer research, the first recognized target in liquid biopsy was circulating tumor cells (CTCs).^[20-22] As a part of tumor tissue, they represent the primary tumor, so their isolation satisfies the objective of biopsy. Although, circulating tumor DNA (ctDNA) is now considered the most important target in liquid biopsy, CTCs are still an attractive target because they carry the full set of tumor-related content and information, including tumor DNA. However, the development of CTC technologies have been stagnant since CellSearch[®] was approved by the FDA in 2008 as the clinical relevance still remains unclear.^[23-25] Most recent methodologies, which preferentially focus on capturing and enumerating CTCs, are complex and are unsuitable for point-of-care diagnosis.^[26-27]

Unlike CTCs, circulating exosomes are stable and abundant in liquid, making them optimal for both quantitative and qualitative clinical studies. Their role is has not yet been clearly defined, but many researchers believe they carry important cargo to even distant organ sites, which is implicated in signaling processes. This means that tumor-derived exosomes may also carry tumor-related content and information, hence playing a significant role in metastasis, just like CTCs. However, due to the lack of functional methods to isolate exosomes in point of care settings, clinical use of exosomes has been hampered. Additionally, as the characteristics (size, shape,


[a] Dr. Y.-T. Kang,⁺ B. Rupp, E. Purcell, T. Hadlock, Prof. S. Nagrath
Department of Chemical Engineering, Biointerface Institute, and Rogel
Cancer Center, University of Michigan, 2800 Plymouth Road,
NCRC B10-A184, Ann Arbor, MI 48109, (USA)
E-mail: snagrath@umich.edu

[b] Dr. Y.-T. Kang,⁺ B. Rupp, E. Purcell, T. Hadlock, Prof. S. Nagrath
Rogel Cancer Center, University of Michigan, Ann Arbor, MI, 48109 (USA)

[c] Y. J. Kim⁺
Department of Nanoengineering, University of California San Diego, La
Jolla, CA 92093, (USA)

[d] Dr. N. Ramnath
Department of Internal Medicine, University of Michigan, Ann Arbor, MI,
48109 (USA)

[⁺] These authors contributed equally to this work

 Supporting information for this article is available on the WWW under
<https://doi.org/10.1002/anse.202100016>

frequency, surface protein expressions, etc.) of CTCs and exosomes are completely different, methods to isolate each circulating biomarker differ from each other. A major drawback for deployment of a one-size-fits-all platform that achieves multi-level detection is a lack of compatibility between platforms tailored to isolate different circulating biomarkers. Therefore, one strategy to address this imbalanced development of technologies is the simultaneous detection of two or three different circulating biomarkers in identical liquid samples obtained from the same patient, allowing complementary readouts from individual biomarkers.

Here we propose a simple, versatile, material-based device-free assay for the simultaneous detection of circulating biomarkers using immunoaffinity-based degradable hydrogel beads (^{LB}beads). Hydrogel beads have been applied to various biological fields, including drug delivery, wound healing, tissue engineering, cell-block formation, etc.; however, use in direct liquid biopsy applications with in-depth studies of its stability as well as degradability was rarely studied. The present beads

overcome the aforementioned issues by using: (a) a highly specific, affinity-based approach to isolate different targets in a single platform; (b) degradable robust hydrogel beads to provide a simple and versatile environment for isolation while also enabling stimuli-driven circulating marker release. Here, we used alginate and poly(vinyl alcohol) (PVA) hybrid hydrogel, that has been mostly used to fabricate cell-laden hydrogel for certain specific applications, such as neocartilage formation for tissue restoration,^[28] wound healing material with mechanical strength,^[29–30] 3D-bioprinting bone tissue scaffolds^[31] due to its greater robustness. We make use of these functional unique characteristics to achieve both highly stable and stimuli-driven degradable functionalities. The beads are formed by ionic gelation and are degraded upon chelating divalent cations (Figure 1A) thus, the captured circulating biomarkers are subsequently released by ion-chelating agent-assisted hydrogel degradation. In this way, the collection of the purified circulating biomarkers from a few drops of blood can be accomplished within 2 hours, including pre-treatment and final

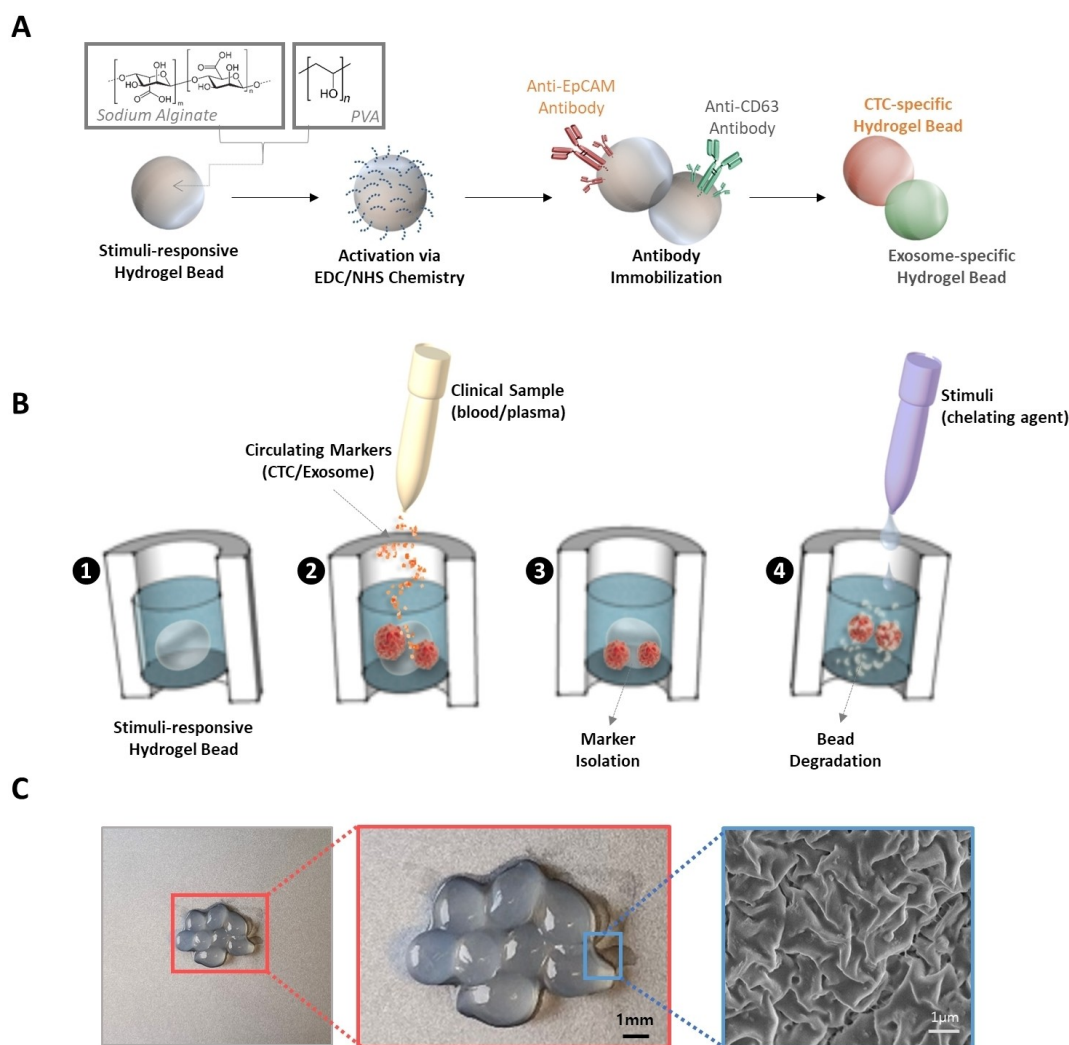


Figure 1. A fabrication and analytical procedure for liquid biopsy using stimuli-responsive hybrid hydrogel beads. **A)** Fabrication of and modification of the liquid biopsy hydrogel to isolate circulating tumor cells (CTCs) and circulating exosomes; **B)** Reaction and procedure of circulating biomarkers isolation and subsequent recovery; **C)** The fabricated liquid biopsy hydrogel beads.

biomarker collection steps (Figure S1). Previously, we devised a microfluidic dual-isolation platform that isolates CTCs and circulating exosomes in melanoma,^[32] however, it still needs sophisticated chemical strategy to release isolated circulating markers from the device and is not easy to scale up to potential larger volumes due to the device saturation. The proposed concept has the advantage of being able to detect multi-level analytes, both CTCs and circulating exosomes (Figure 1B) and easily release them via stimuli-driven hydrogel release. Its relatively cheap price and easy scale-up possibility also allows for larger volume processing. Preclinical studies using model samples containing cancer cells or cancer cell-derived exosomes demonstrated that the present hydrogel beads functionalized with specific antibodies are capable of target circulating biomarker recovery. We extended our study to clinical blood samples from patients with non-small cell lung cancer (NSCLC) to illustrate the translational potential of the present platform, and we showed that not only each biomarker isolation from blood but also potential translational implications in dual-circulating biomarker isolation towards cancer diagnosis. To the best of our knowledge, this is the first hydrogel platform being able to isolate multiple circulating markers from clinical samples in various buffer/reagent conditions. This versatile platform and comprehensive profiling of circulating biomarkers will allow for enhanced understanding of diseases.

Results and Discussion

Preparation of hybrid hydrogel beads for circulating biomarker isolation

An important advantage of this hydrogel-based approach is biocompatibility. As hydrogels are composed of a crosslinked polymeric network, they have the innate capacity to hold water within their porous structure,^[33] providing a native-mimicking environment different from rigid artificial environments. Due to their high water absorbing capacity, hydrogels have been applied to a host of biological challenges, including 3-dimensional cell culture,^[34] microencapsulation,^[35] tissue engineering,^[36] wound healing,^[37] drug delivery systems,^[38,39] cell block formation,^[40] biosensors and bioelectronics.^[41,42] However, it is difficult to achieve both degradability and chemical stability in common hydrogels since those requirements are somewhat entangled. Classically, degradability is a property of “physical hydrogels” (also known as “reversible hydrogel”), that commonly prohibits long-term incubation with biological samples. Whereas chemical stability is a property of “chemical hydrogels” (also known as “permanent hydrogel”), which are not suitable for short-term application. Recently, a few researchers have blended more than one type of hydrogel using various physical or chemical cross-linking methods for their own applications,^[43,44] and here, to achieve our goal of having both of these properties, we blended two hydrogels: alginate (biodegradable natural hydrogel) and PVA (chemically stable synthetic hydrogel). The present beads, composed of the two-component hydrogels, have the stability to endure bio-

logical solutions for extended durations, and can be naturally degraded in a short time with application of specific stimuli. The fabricated hybrid hydrogels are in millimeter scale ($d = 2.21 \pm 0.30$ mm) and shown in Figure 1C.

Stability of the hybrid hydrogel beads

In order to evaluate the applicability of the present hydrogel platform to isolate circulating biomarkers in various buffers and solutions, we examined the pH responsiveness, stability, and degradability of the hybrid hydrogel. Figure 2 shows the basic characterization of the hybrid hydrogel when exposed to various buffered solutions, cell culture media, or chelating solution. Average initial and dehydrated weight of the beads were 4.45 ± 0.06 mg and 0.22 ± 0.01 mg, respectively ($n = 90$), and the shrink-swell ratio was calculated at 20.23 ± 0.02 . The shape and weight of the beads were preserved for multiple days with minimal degradation and significant changes were not apparent even after 10 months of incubation (Figure S2 and Figure S3). During the incubation period ($t = 120$ minutes), the weight had varied approximately 4~8% from their initial values (Figure 2A). Given that the beads were quite swollen at the initial state ($t = 0$ minutes), the beads were thoroughly stable in the buffered solution: weight change % of $6.42 \pm 1.77\%$ (Sodium acetate, pH 5.0); $5.50 \pm 1.20\%$ (MES, pH 5.5); $5.83 \pm 1.79\%$ (Sodium citrate, pH 6.0); $5.96 \pm 0.67\%$ (MOPS, pH 6.5); $4.68 \pm 1.05\%$ (PBS, pH 7.0); $4.25 \pm 0.16\%$ (HEPES, pH 7.5); $6.28 \pm 1.55\%$ (Tris-HCl, pH 8.0); $7.52 \pm 2.68\%$ (Sodium borate, pH 8.5). From these results, we interpret the pH-responsive behavior as follows. (a) In an acidic environment, the hydrogel beads lost the water stored inside, followed by slight shrinking. As a result, the rate of change in weight increased without regard to the original structure and composition. (b) In a basic environment, the hydrogel beads absorbed the water from outside, and were gradually swollen; but it is hard to preserve their original structure because they were loosely bonded through ionic interaction. Consequently, the beads were slowly damaged. The results from incubation with cell culture media also support our expectation (Figure 2B). Although they were exposed to a cation-rich environment, the weight change rate observed in the first 120 minutes did not differ significantly with other buffered solutions: $5.72 \pm 0.58\%$ (DMEM); $6.59 \pm 0.51\%$ (MEM); $6.34 \pm 0.83\%$ (RPMI 1640). When considering that the weight change rate against cross-linking solution was also estimated to be $2.21 \pm 2.39\%$, the beads were still stable in the cell culture media. On the other hand, the beads were substantially degraded after 60-minute incubation with chelating solutions: $75.54 \pm 4.74\%$ (EDTA); $65.78 \pm 5.16\%$ (EGTA); $60.88 \pm 0.00\%$ (BAPTA); $29.03 \pm 3.88\%$ (IDA); $47.77 \pm 3.89\%$ (NTA); $73.27 \pm 12.21\%$ (DTPA). The differences in degradation rate between the six chelators were related to their own equilibrium constant against calcium ions. The beads in the EDTA and DTPA groups were too pulpous to handle at this point, thus 120-minute follow-up was impractical because they had almost disappeared. As we expected, EDTA was most effective in degradation of the present beads

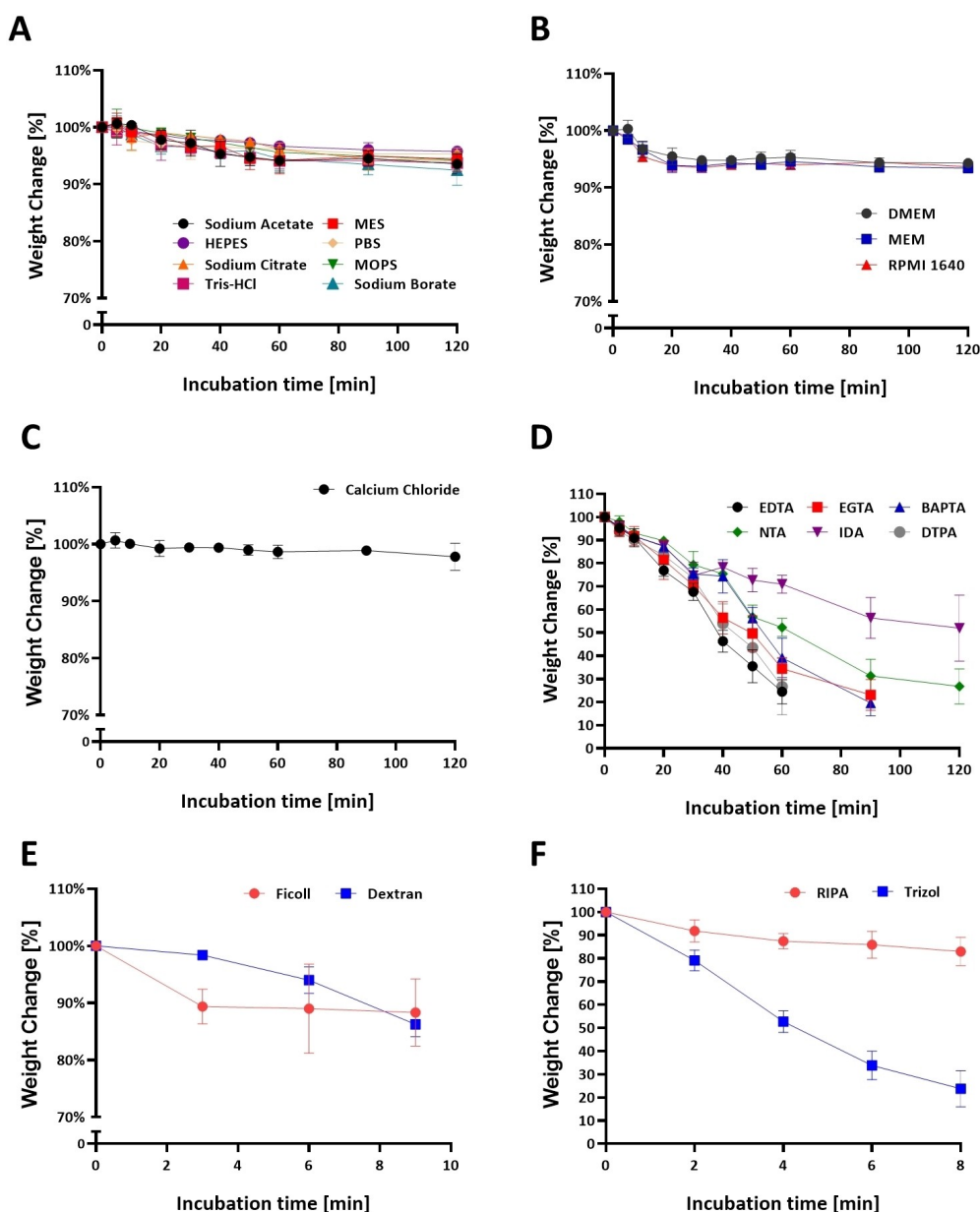


Figure 2. Basic characterization of the stimuli-responsive hydrogel beads consisting of poly(vinyl alcohol) and alginate. **A)** Stability of the present hydrogel beads against 8 biological buffers varying pH level (Sodium acetate (pH 5.0), MES (pH 5.5), Sodium citrate (pH 6.0), MOPS (pH 6.5), PBS (pH 7.4), HEPES (pH 7.5), Tris-HCl (pH 8.0), Sodium borate (pH 8.5)); **B)** Stability of the present hydrogel beads against 3 widely used cell culture media (Dulbecco's Modified Eagle's Medium (DMEM), Minimum Essential Medium (MEM), Roswell Park Memorial Institute (RPMI) 1640 medium); **C)** Stability of the present hydrogel beads against crosslinking solution (calcium chloride); **D)** Degradability of the present hydrogel beads against 6 chelators having different stability constant (ethylenediaminetetraacetic acid (EDTA), ethylene glycol tetraacetic acid (EGTA), (1,2-bis(*o*-aminophenoxy)ethane-*N,N,N',N'*-tetraacetic acid) (BAPTA), iminodiacetic acid (IDA), nitrilotriacetic acid (NTA), and diethylenetriaminepentaacetic acid (DTPA)); **E)** Stability of the hydrogel beads against two different plasma separation reagents; **F)** Degradability of the present hydrogel beads against two different lysis buffers, RIPA and Trizol, for protein and nucleic acid extraction, respectively.

(Figure 2D). In order to apply the beads to pre-separated layers of blood, we examined the beads stability in two different plasma separation reagents, Ficoll-Paque and 6% dextran solution (Figure 2E). The beads did not show any noticeable change in weight up to ten minutes, implying possibilities for direct use of the beads in plasma or buffy coat layer. Given the need for isolated cell/vesicles to undergo further downstream analysis, we evaluated the bead stability in two different cell/vesicle lysis buffers, RIPA and Trizol (Figure 2F). The beads

remained stable in RIPA for more than five minutes, which is enough to lyse cells/vesicles while beads in Trizol showed notable weight loss after two minutes of incubation. As RIPA buffer is used for membrane lysis of EVs for protein analysis, we performed protein marker expression studies using recovered exosome samples.

Evaluation of ^{LB}Beads for circulating biomarker isolation using model samples

We then modified the stimuli-responsive hydrogel beads with various antibodies to isolate circulating biomarkers in blood. Based on their intended target biomarker, each sub-type of beads was classified as either CTC beads (anti-EpCAM antibody-immobilized hydrogel beads) or exosome beads (anti-CD63 antibody-immobilized hydrogel beads). Meanwhile, WBC beads (anti-CD45 antibody-immobilized hydrogel beads) and unmodified beads without antibody conjugation were prepared as non-target and blank controls, respectively. Each sub-type of beads was then incubated with model samples containing breast cancer cell line MCF-7 derived circulating biomarkers in buffer solutions. The performance of the beads was evaluated using fluorescence-based relative target biomarker affinity, capture efficiency, immunofluorescence staining analysis, and electron microscopy analysis.

First, we performed CTC isolation and characterization studies with CTC beads, WBC beads, and control beads. Each sub-type of beads was incubated with CTC model samples containing spiked cancer cells and WBCs in PBS buffer solution. After a 60-minute incubation, recovered beads were stained with FITC-conjugated anti-EpCAM antibody and TRITC-conjugated anti-CD45 antibody. Then, we compared the FITC-fluorescence intensity of the CTC-specific beads to that of the WBC and control beads (Figure 3A) using fluorescence microscopy. The results show the average fluorescence signal intensity of CTC beads ($n=5$) was 1.92 times higher than that of the control beads ($n=5$). The level of intensity was evenly distributed among all five beads. Although the fluorescence

signal intensity of WBC beads ($n=5$) was greater than that of the control beads, wide variation existed amongst beads, which we attributed this signal to non-specific binding of cancer cells or 1–10% unavoidable fluorescence overlap from WBC staining with TRITC. In order to evaluate the specificity of each bead type, we incubated our beads in prepared CTC and WBC model samples containing a known number of spiked cells. As a result, CTC beads showed a 28.1-fold increase in captured cancer cells compared to the unmodified beads; on the contrary, approximately 24.5 times more WBCs were isolated by WBC beads than CTC beads, at the identical condition. The cell loss due to nonspecific binding was estimated to be less than 2 cells per bead. This result implies that our CTC beads specifically isolate CTCs from a heterogeneous sample without significant cell loss.

To evaluate a CTC capturing performance of the beads, we spiked a known number of cells (~200 cells) into blood/PBS buffer, applied to our 8–10 CTC-beads, recovered the beads, and dissolved them in EDTA solution for 10 minutes for captured cell enumeration on Cytospin slides. At the same time, control beads having no antibody conjugation were also applied to identical samples and compared with CTC beads. From this study, we found that a significantly higher number of cancer cells are captured using CTC beads (Figure 3B, Figure S6) at both cancer cells spiked in buffer and blood samples. Quantitatively, over 30% of spiked cancer cells were recovered using CTC-beads while control beads captured less than 5%. This specific cell isolation ability was also evaluated using a fluorescence microscope (Figure 3C) and a Field Emission Scanning Electron Microscope (FE-SEM) (Figure 3D). Pre-fluoresced cancer cells were successfully recovered using CTC beads. The hydrogel beads showed sub-microscale wrinkling patterns

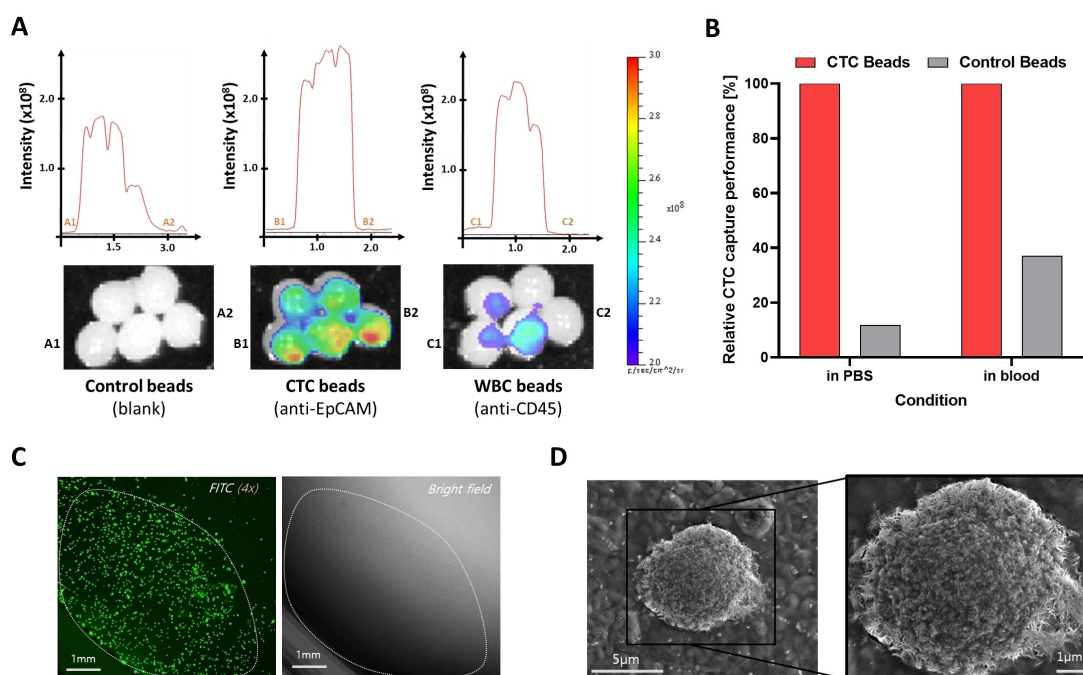


Figure 3. Performance of liquid biopsy hydrogel beads (^{LB}Beads) for circulating tumor cell (CTC) recovery. **A**) CTC capture performance comparison based on fluorescence intensities using fluorescent cancer cells with three different hydrogel beads; **B**) CTC recovery performance after capture and release cancer cells from the beads; **C–D**) Isolated fluorescent MCF-7 cancer cells under fluorescence microscope (**C**) and scanning electron microscope (SEM) (**D**).

due to the methodology of the gelation process (Figure 3D); thus, the image of the captured circulating biomarkers can be distinctly distinguished on the basis of size and shape.

Simultaneously, exosome-specific beads were separately incubated with exosome model samples made from MCF-7 cancer cell culture supernatant. After a 60-minute incubation, the performance of exosome-specific beads was assessed in the same manner as CTC beads, utilizing fluorescence imaging, nanoparticle tracking analysis, bicinchoninic acid (BCA) analysis, and electron microscopy study. Implementing a similar fluorescence comparison study, we found that the exosome beads (anti-CD63) (Figure 4A) showed 3.26 times higher average EpCAM fluorescence signal intensity compared to the unmodified beads. More important implications of this data are shown in the results from exosome-specific beads incubated with exosome-free samples. The average signal intensity of exosome beads incubated in exosome-free buffer was similar to that of the unmodified beads, but significantly lower than that seen with exosome-specific beads incubated with exosome samples. These results show that: (a) the MCF-7 cell derived-exosomes are successfully isolated by the Exosome-specific beads and; (b) the MCF-7 cell derived-exosomes show EpCAM expression, just like the cells of their origin.

For capture efficiency of exosome beads, we used two different analysis methods, nanoparticle tracking analysis and BCA analysis. Starting from a known concentration of exosomes ($\sim 6.0 \times 10^9/\text{ml}$), we compared exosomal concentrations before and after isolation on the beads. From this study, we found that exosome beads capture over 60% of spiked exosomes

while control beads capture less than 20% of spiked exosomes. We found similar results using BCA analysis measuring total protein quantity after exosome isolation and lysis (Figure 4B). Exosome beads' specificity was evaluated by a fluorescence microscope and an electron microscope. Exosomes pre-stained with lipophilic dye were identified on exosome beads surface (Figure 4C). The exosomes on exosome beads were easily distinguished since the size of the vesicle (50~100 nm) was much smaller than that of wrinkling patterns on the surface; as a consequence, the inherent structures remained, but were also covered by a large number of exosomes (Figure 4D).

Dual-circulating biomarker isolation using clinical samples from non-small cell lung cancer patients

We tested the feasibility of this application to process and analyze samples from cancer patients. Recent reports suggest that there may be value in obtaining complementary data from two or more circulating biomarkers in the blood as a way to provide more comprehensive analysis in patients with cancer. Recent work analyzing both cell-free DNA (cfDNA) and exosomal RNA showed meaningful progress in rare mutant detection by qPCR and next generation sequencing (NGS) compared to analyzing cfDNA alone.^[45] Y.-J. Chiu et al. analyzed the cancer cells and cancer cell derived exosome in terms of single cell analysis under various physical/chemical stimuli. However, this study only focused on a model sample so clinical

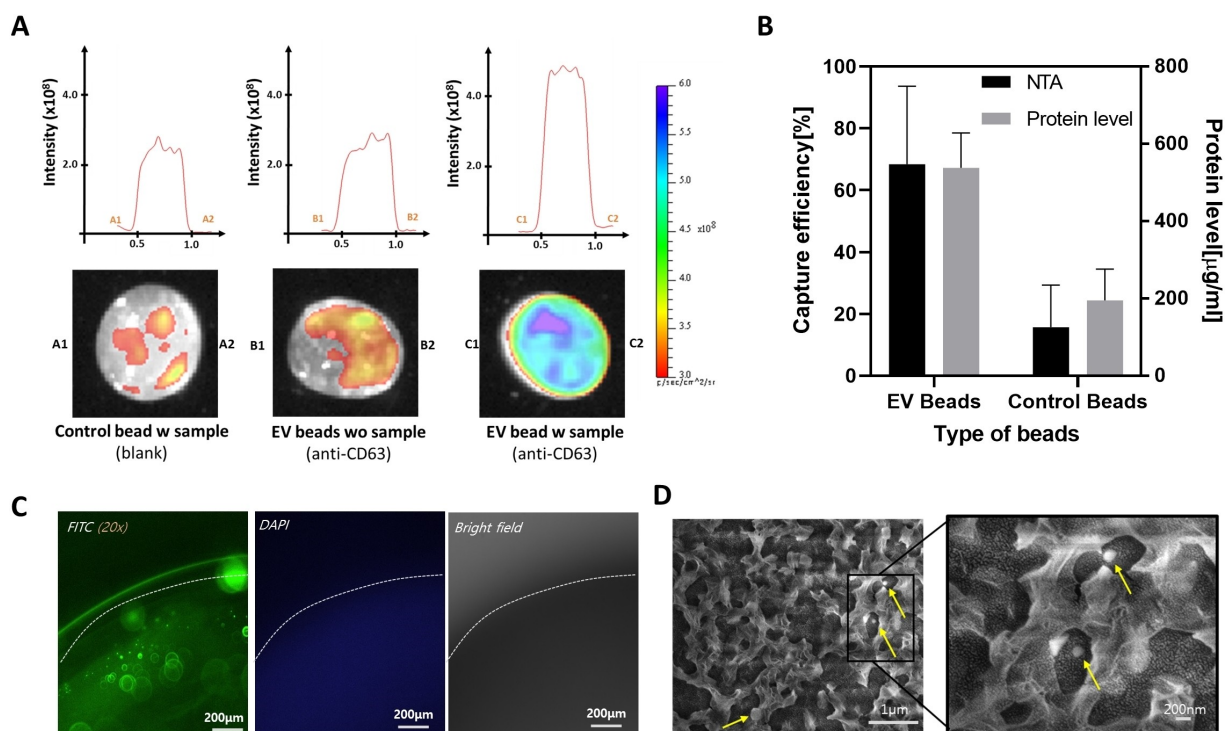


Figure 4. Performance of liquid biopsy hydrogel beads (^{LB}Beads) for exosome recovery. **A**) Exosome capture performance comparison based on fluorescence intensities using exosome fluorescence staining; **B**) Exosome recovery performance based on nanoparticle tracking analysis (NTA) and total exosomal protein quantities; **C–D**) Isolated and lipophilic dye stained MCF-7 derived exosomes under fluorescence microscope (**C**) and scanning electron microscope (**D**).

studies using several circulating biomarkers have not been successfully accomplished yet.^[46]

Here, we chose two types of beads, CTC-specific bead and exosome-specific bead, to capture and study two types of biomarkers using identical blood samples from the same patients. Five clinical samples from non-small cell lung cancer (NSCLC) patients and 3 healthy donor blood samples were tested. Whole blood samples were separated into two samples, buffy coat and plasma layer, and used for CTC and exosome isolation, respectively.

For CTC isolation, given that NSCLC cancer cells express EGFR as well as EpCAM, combined antibody cocktails were used to make CTC-specific beads. The beads were incubated with cell samples, and after 1 hour incubation we decomposed the CTC-specific beads ($n = 10$) using an EDTA solution, and the

isolated CTCs were then collected by centrifugation. Remaining cells were cytopun onto glass microscope slides and fluorescently stained for four unique cell markers: DAPI, CD45, pan-cytokeratin, and vimentin. DAPI+/cytokeratin+/CD45- cells were considered as CTCs. Vimentin positivity was considered as a mesenchymal property of CTCs. As shown in Figure 5A, an average 37.4 ± 30.7 CTCs were found in 1 milliliter of patients' blood from the five different NSCLC patients. Also, NSCLC patient samples contained significant concentrations of CTCs in all samples tested, while only 1 healthy donor sample contained any CTCs. This is significant as an increased number of CTCs in NSCLC patients has been linked with poor prognosis.^[47,48] The robustness of our platform was also compared to our in-house label-free microfluidic device, Labyrinth (Figure 5B).^[49,50] As ^{LB} beads isolate CTCs via immu-

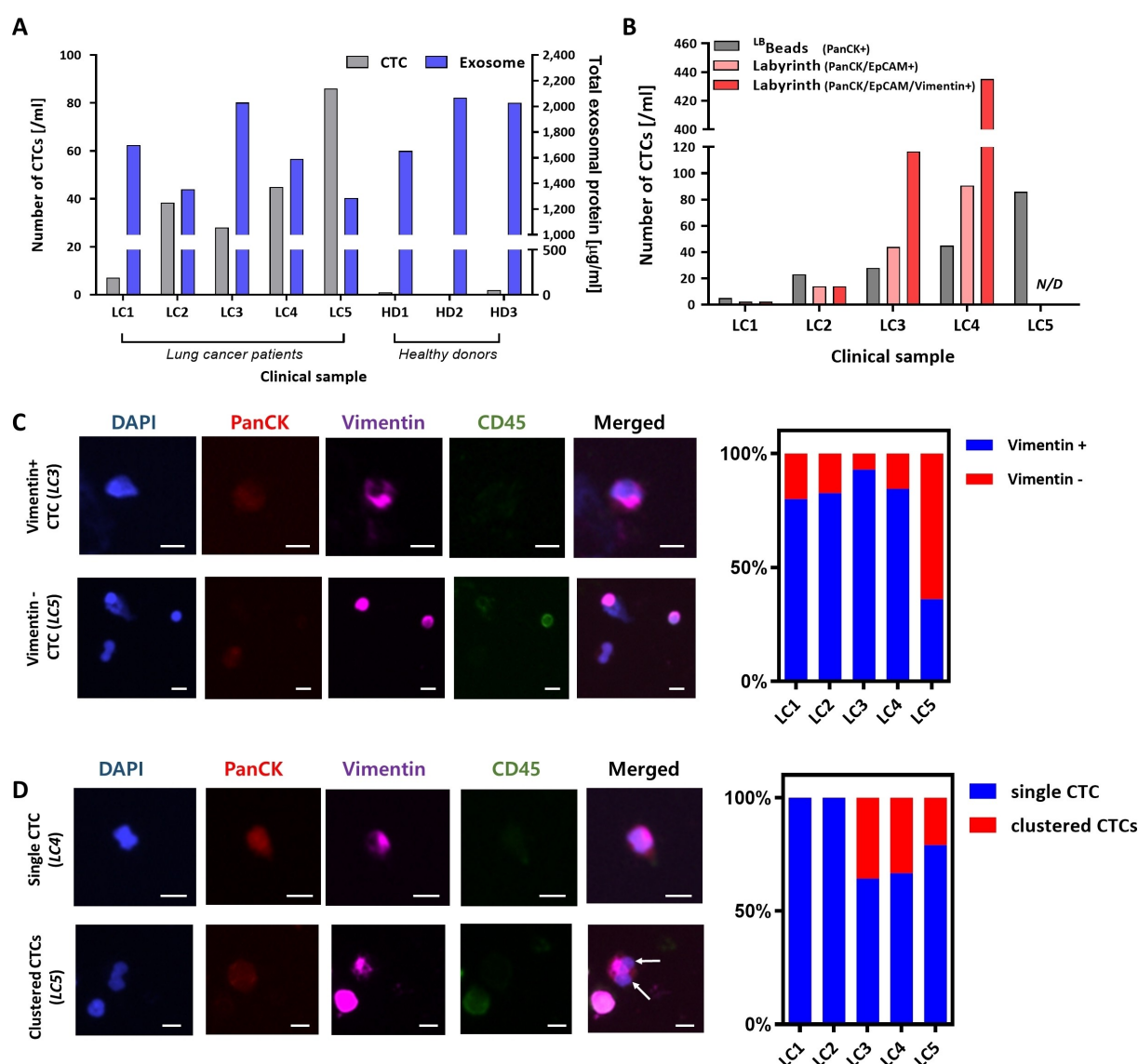


Figure 5. Profiling of circulating biomarkers in non-small cell lung cancer patients' blood. **A**) Circulating biomarker quantity analysis using immunostaining (CTCs) and BCA analysis (Exosome); **B**) CTC isolation performance comparison between ^{LB} beads and label-free CTC isolation microfluidics, Labyrinth; **C**) Vimentin expression analysis of CTCs isolated from lung cancer patient blood samples; **D**) CTC cluster analysis of CTCs isolated from the same lung cancer patient samples (All scale bars = 10 μm). Arrows identifying the CTC cluster in LC5 merged image.

noaffinity-based isolation as does the only FDA-approved CTC technology, CellSearch, we compared CTC isolation performance with a size-based CTC isolation device. When we compared with Pan CK+/EpCAM+ cells isolated by Labyrinth, our device-free platform showed a competing result with an average CTC number of 37.4 CTCs/ml vs. 30.2/ml from Labyrinth for 5 lung cancer clinical samples. However, due to the principle of CTC isolation we used, our platform might miss certain subtypes. For example, LC4 had more than 300 CTCs that are exclusively vimentin positive, yielding a huge discrepancy between two methods. More detailed profiling of these CTC subsets using a label-free CTC isolation is described in Figure S7. This can be further improved by immobilizing new antibodies to our hydrogel beads. It is also noteworthy that our platform isolates more CTCs than the label-free isolation device in some cases. As the label-free device makes use of size difference between CTCs and WBCs, it is possible that smaller sized CTCs might have been missed during the sample processing while our immunoaffinity-based platform isolates them without any difficulty.

CTCs from cancer patients include cytokeratin positive cells that were vimentin-positive and vimentin-negative, and more than 75.2% of cells were verified as dual-positive. On a case-by-case analysis, we found noticeable differences among the patients: (a) CTCs recovered from most samples express a predominant amount of vimentin; (b) over 50% of captured CTCs in LC5 are vimentin negative. The representative images of this heterogeneity in CTCs are shown in Figure 5C (left).

Vimentin expression amongst CTCs isolated from each patient was then examined, with results shown in Figure 5C (right). These results show that in 80% of patients tested, a majority of isolated CTCs were vimentin positive. The high expression of vimentin, an EMT marker, has been demonstrated on CTCs isolated from NSCLC patients, and has been linked to liver metastasis.^[47,51]

The existence of CTC clusters within patient blood samples was investigated. As shown in Figure 5D, 60% of tested patient samples contained CTC clusters. Clustered CTCs accounted for almost 30% of all isolated CTCs within patients' samples containing at least one CTC cluster.

Concurrently, we analyzed the exosome-specific beads in two different ways: (1) exosomal protein analysis using BCA for quantitative analysis of exosome and (2) western blotting analysis for qualitative analysis of exosomes. For both cases, we directly applied RIPA lysis buffer to extract proteins. At the same time, we also isolated exosomes using a gold-standard exosome isolation technique, ultracentrifugation and analyzed their quantities using a widely-used exosome quantification method, NanoSight. The overall results from a nanoparticle tracking analysis (NTA) and a protein quantity study in 8 different clinical samples are summarized in Figure 6A. It is noteworthy that in overall cases, the trend of total protein quantities between samples is similar as that from ultracentrifugation, which is analyzed using NanoSight. From the comparison between quantities in CTC and exosome within samples, there were no differences in total quantity (Figure 5A).

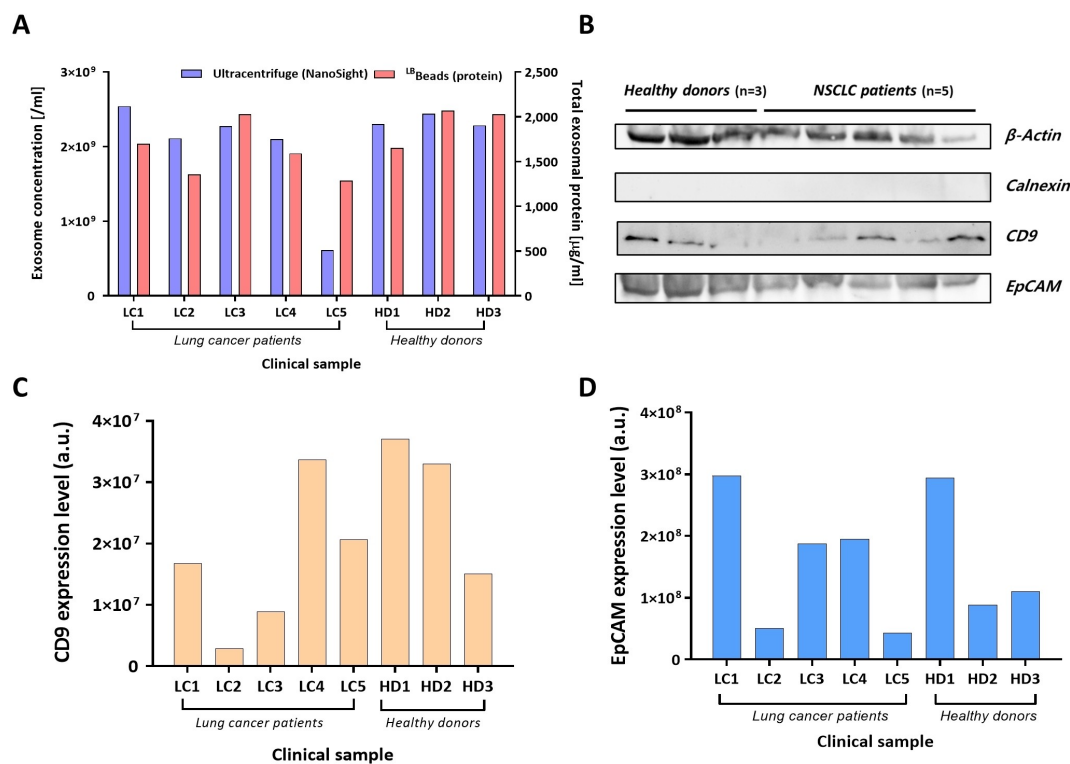


Figure 6. Profiling of exosomes in non-small cell lung cancer patients' blood. A) Comparison of the exosome recovery between ultracentrifugation (analyzed by NanoSight) and ¹⁵Beads (analyzed by total protein concentration) using clinical samples; B) Western blotting analysis of exosomes in clinical samples; C–D) Exosomal (C) and epithelial cancer marker (D) relative expression on isolated exosomes from clinical samples.

However, percentage of vimentin positive CTCs may be related to total exosome protein quantity, implying that mesenchymal CTCs secrete more exosomes though further studies are needed to verify this claim. Also, no significant difference in exosome concentration was observed between patients and healthy donors even though healthy donors showed higher quantities compared to that of cancer patients. In order to study innate information of exosomes, we performed western blotting analysis and quantified certain protein expressions based on blot images. Western blot images (Figure 6B) revealed that recovered exosomes express exosomal protein marker, CD9, while a cellular marker, calnexin, shows negative, implying that the Exosome-beads is capable of exosome isolation with high specificity and purity. The western blots were run using Bio-rad's Stain Free Gel system, whereby each specific proteins band can be normalized to the total protein of its lane. This allowed us to compare the relative protein expression of both CD9 and EpCAM between samples (Figure 6C–D). This study revealed that healthy donor group shows 1.71 times higher expression in CD9. There is no difference in EpCAM expression between cancer and healthy in spite of its significance in CTC studies. This is likely because exosomes derive from all cell types, including many epithelial cell types, which would lead to a fairly consistent EpCAM expression between people.

From these studies, one could glean a few conclusions that will need verification in larger studies. First, as we evaluated in a recent study, there was no significant relationship between number of CTCs and concentration of total exosomes.^[52] However, we noted a direct correlation between the fraction of CTCs expressing mesenchymal markers and total exosome concentration; this is similar to what has been previously reported.^[52] Second, results from one biomarker correlated to data on other biomarkers, demonstrating a major advantage of simultaneous detection of two biomarkers from the same patients. As shown in Figure 5A, CTC enumeration alone would not be a convincing metric for *LC1* because the CTC count was relatively low comparing to healthy controls. However, EpCAM expression in exosomes from *LC1* is relatively higher compared to others and could therefore serve as a complementary biomarker. As exosome quantity and detection frequency is generally higher than that of CTCs, this dual-marker analysis could allow for a better understanding about disease. More work with a larger clinical cohort will be needed to make more robust comparison and definite conclusions.

It is also possible that our technology could be compared to conventional magnetic bead-based isolations or microfluidic devices that have been used in liquid biopsy. However, the present hydrogel platform offers very affordable cost of analysis, easy circulating marker release, minimized antibody use, and ferrofluid-free condition for further potential downstream analysis.

Our research might have several drawbacks, some pertaining to inherent limitations associated with circulating biomarker isolation. As our CTC-specific beads have more affinity to epithelial-like CTCs, our approach may miss some portion of CTCs which have lost EpCAM or EGFR expression during EMT process. Since the frequency of mesenchymal-like CTCs in

circulation is not fully revealed, discrepancies in total epithelial CTC number and cancerous exosome concentration could be increased as disease complexity increases. For example, relatively low numbers of CTCs and relatively high exosome concentration for *LC1* may be explained by the patient's tumor displaying more mesenchymal characteristics.

Similarly, there might be difference in mesenchymal protein expression between CTCs and exosomes. *LC5* showed the highest epithelial characteristic in CTCs having the lowest percent of vimentin positivity, however its associated exosomes showed low expression of EpCAM.

In the following future study using the current platform, we will consider several facts recently discovered to analyze our data in more detail. 1) Circulating tumor cells from patients with advanced cancer display both epithelial and mesenchymal markers.^[53] 2) Mesenchymal stem cells secrete more exosomes than epithelial cancer cell.^[52] We expect that further findings and studies involving larger groups of patients would uncover unsolved results from this study.

Conclusion

In summary, we created a hybrid hydrogel and applied our hydrogel-bead platform for blood-based liquid biopsy using two circulating biomarkers. The stimuli-responsiveness of the present hydrogel facilitates the capture and release of circulating biomarkers using immunoaffinity technology. The versatility of the present platform allows for simultaneous isolation of two circulating biomarkers, CTCs and exosomes, from NSCLC patient blood samples, with a simple alteration of antibodies. Using the present platform, we were able to comprehensively diagnose the status of patients using two circulating biomarkers, allowing complementary readouts from individual biomarkers. To the best of our knowledge, this study is the first report on a device-free platform aiming to isolate dual circulating biomarkers in identical samples and finding the similarities and differences between them. We hope that the comprehensive results from the present novel liquid biopsy platform would enable us to get a better understanding of disease that may eventually aid in simple clinical decision making.

Experimental Section

Materials and reagents: 99.5% ethyl alcohol, sodium alginate (brown algae, low viscosity), poly(vinyl) alcohol (Mw 85,000–124,000), calcium chloride, 1-ethyl-3-[3-dimethylaminopropyl] carbodiimide (EDC), and N-hydroxysulfosuccinimide (Sulfo-NHS) were purchased from Sigma-Aldrich (St Louis, MO). Dulbecco's Modified Eagle Medium (DMEM), Minimum Essential Medium (MEM), Roswell Park Memorial Institute (RPMI) 1640 medium, 1% (v/v) penicillin–streptomycin, and 10% (v/v) fetal bovine serum were purchased from Invitrogen (Carlsbad, CA) and Gibco (Gaithersburg, MD). Avidin, biotinylated BSA, CellTracker™ Green CMFDA were purchased from Thermo Fisher Scientific (Waltham, MA). Biotinylated anti-EpCAM antibody and Biotinylated anti-CD63 antibody

were purchased from BD bioscience (San Jose, CA). All chemicals were used as received.

Fabrication of the degradable hydrogel beads: The degradable hydrogel beads were prepared as follows. First, 2% (w/v) alginate solution and 2% (w/v) PVA solution were blended under constant stirring at 85 °C, followed by cooling down to room temperature. In the meantime, the aggregated pellets inside the mixture were whisked vigorously using homogenizer until completely disappeared. Then, the homogenized, hybrid mixture composed of two hydrogels were left to age for more than 48 hours. Separately, crosslinking solution was prepared by diluting calcium chloride (CaCl₂) solution to deionized water in a 1:10 volume ratio. Afterwards, the prepared mixture was loaded in a form of droplets into a crosslinking solution through a homemade extruder; each hydrogel drop was solidified instantaneously as a spherical shape. Finally, the fabricated beads were further incubated with crosslinking solution for hardening their structure.

Characterization of the degradable hydrogel beads: The prepared degradable hydrogels were evaluated based on size, weight, shrink-swell ratio, chemical stability, and degradability. First, the diameter and weight of the beads were measured using metric ruler and laboratory scales. Then, the beads were submerged into deionized water and incubated for 24 hours, followed by size and weight measurement. The same procedure was repeated when the beads were completely dehydrated after natural drying for 24 hours. Based on the shift in weight, shrink-swell ratio was estimated as follow:

Shrink – Swell Ratio =

$$\frac{(\text{The weight of fully – hydrated hydrogel bead})}{(\text{The weight of dehydrated hydrogel bead})}$$

Stability of the degradable hydrogel beads: The stability of the present hydrogel was evaluated by incubating with the most widely used buffer solution with different pH level: Sodium acetate (pH 5.0), MES (pH 5.5), Sodium citrate (pH 6.0), MOPS (pH 6.5), PBS (pH 7.0), HEPES (pH 7.5), Tris–HCl (pH 8.0), Sodium borate (pH 8.5). Considering their inherent pH range, each solution was chosen and adjusted to the precise pH level using 5% acetic acid and 1 mM NaOH. Second, the stability against three kinds of cell culture media was investigated: Dulbecco's Modified Eagle's Medium (DMEM), Minimum Essential Medium (MEM), Roswell Park Memorial Institute (RPMI) 1640 medium. The evaluation was performed on the basis of the percent of weight change during the fixed incubation time (5 min, 10 min, 20 min, 30 min, 40 min, 50 min, 60 min, 90 min, and 120 min). The stability of hydrogels against two widely known cell lysis reagents for downstream analysis was also investigated: RIPA for protein extraction and Trizol for nucleic acid extraction. At last, the stability against two plasma separation reagents was evaluated: Ficoll and Dextran. For increasing consistency and decreasing variability, each bead at a certain period was taken out of the test tube and pat dried thoroughly with clean wipers, and then weighted using laboratory scale. The measurement in each condition was repeated five times with five different beads.

Degradability of the degradable hydrogel beads: The degradability of the present hydrogel was evaluated by incubating with six different kinds of chelating agent: ethylenediaminetetraacetic acid (EDTA), ethylene glycol tetraacetic acid (EGTA), (1,2-bis(o-aminophenoxy)ethane-N,N,N',N'-tetraacetic acid) (BAPTA), iminodiacetic acid (IDA), nitrilotriacetic acid (NTA), and diethylenetriaminepentaacetic acid (DTPA). The six candidates were chosen based on stability constant and reactivity to mono-, di-, or trivalent cation. Since these molecules scavenge divalent cations, mostly Ca²⁺ in

here, the ionically crosslinked fibers were gradually separated from outer to inner space of the beads. As a result, the weight of the beads decreased with the incubation time (10 min, 20 min, 30 min, 40 min, 50 min, 60 min, 90 min, 120 min). Alike stability test, each bead at a certain period of time was taken, pat dried, and weighed five times for increasing consistency and decreasing variability.

Surface modification and antibody immobilization: The antibodies were immobilized onto the prepared hydrogel beads following previously reported methods.^[54–56] First, the beads were slightly dehydrated and fully hydrated again using deionized water. Separately, 200 mM of 1-ethyl-3-[3-dimethylaminopropyl] carbodiimide (EDC) and 200 mM of N-hydroxysulfosuccinimide (Sulfo–NHS) were prepared by dissolving in deionized water and mixed in a 1:1 ratio to activate EDC–NHS coupling. Then, the beads were incubated with the mixture under constant stirring at room temperature. Subsequently, the beads were carefully washed with deionized water so as not to damage the soft and swollen surface. Afterwards, the beads containing amine-reactive functional group were immersed in the order as followed: 1 mg/ml of biotinylated BSA solution (in 10 mM Tris buffer); 200 µg/ml of avidin solution (in 10 mM Tris buffer); 1 ~ 10 µg/ml of biotinylated antibody solution (in 10 mM Tris buffer). Each step was conducted at 4 °C, and the unreacted molecules were removed by washing with PBS buffer solution. At the final step of antibody immobilization, the beads were designed differently for the type of antibody: anti-EpCAM antibody, anti-CD45 antibody, and anti-CD63 antibody were chosen for CTC isolation, WBC elimination, and exosome isolation, respectively.

Surface characterization using field emission electron microscope (FE-SEM): The morphology of the modified surface was examined using a Magellan400 (FEI company, USA) attached Schottky thermal field emitter gun (FEG). The images were recorded with the in-lens detector (TLD) at an acceleration voltage of 3.0 kV, by setting a working distance of 4.5 ~ 5.5 mm. The operating condition was optimized in order to minimize sample damage. The bead samples were fixed using 4% formalin solution, washed with PBS buffer, and dehydrated in increasing concentrations of ethanol (70, 80, 90, 95, and 100%) for 5 minutes each. Then, they were cut in half, attached onto SEM stub, and coated with osmium of 3.0 nm thickness for avoiding degradation or charging effects of biomolecules and hydrogels. The purpose of the FE-SEM measurement was: (a) to confirm the surface condition (shape, appearance, porosity, and so on) of the present beads; (b) to confirm the presence of the capture circulating biomarkers or background cells (e.g. white blood cells).

Cancer cell culture and model sample preparation: Two cell lines of breast cancer, MCF-7 and MDA-MB-231 were used in this work. Each cell line represents the epithelial- and mesenchymal-like phenotype in CTCs, respectively. MCF-7 and MDA-MB-231 were cultured in Dulbecco's modified Eagle's Minimal Essential Media (DMEM, Life technologies, Inc.). Media was supplemented with 10% (v/v) exosome-depleted fetal bovine serum (System Bioscience, LLC) and 1% (v/v) penicillin–streptomycin (Invitrogen). For the CTC model samples, we spiked the cancer cells in 1 ml of PBS solution or blood from healthy donors at the cell concentration of 1 × 10⁵ cells/ml. This model sample was used for performance verification of anti-EpCAM antibody conjugated bead for CTC isolation. For the exosome model samples, 1 × 10⁵ number of cancer cells was incubated in exosome-depleted media for 1 day, then cell culture supernatant (CCS) was gently replaced from the cell plate. This CCS was followed by mild centrifugation for excess cell elimination, and then 1 ml of CCS was prepared for performance verification of anti-CD63 conjugated bead for exosome isolation.

Human blood sample preparation: The sample collection and experiments were approved by University of Michigan Institutional Review Board (IRB). Informed consents were obtained from all participants of this clinical study and non-small cell lung cancer blood samples were obtained after approval of the institutional review board at the University of Michigan (HUM00119934). Clinical information of patient samples can be found in Table S2. All experiments were performed in accordance with the approved guidelines and regulations by the ethics committee at the University of Michigan. The blood sample (1mls each) was collected in BD Vacutainer® tube and used within 12 hours after sampling. The blood sample was used without dilution and any pretreatment such as erythrocyte lysis or density gradient separation for minimizing the cell loss during any other processes.

Immunofluorescence staining for circulating tumor cell study: Cells captured by the anti-EpCAM bead were analyzed by immunofluorescence staining. After release of captured cells from the bead, cells were cytospun onto glass slides at 800 rpm for 10 minutes at medium acceleration and subsequently cytospun with 4% paraformaldehyde (PFA) (16% PFA was diluted 1:4 in PBS, Cat.# PI28908, ThermoFisher) for fixation using the same parameters. Glass slides were rinsed with PBS 3 times before being stored at 4°C until multiple samples could be obtained and stained in batch. For staining, slides were permeabilization using 0.2% Triton X-100 (Cat. # T9284, Sigma-Aldrich) for 3 minutes before being rinsed with PBS 3 times for 5 minutes each. Slides were subsequently blocked for 30 min each using a blocking solution of 1% bovine serum albumin (Cat.# B4287, Sigma-Aldrich) and 10% normal goat serum (Cat.# 50062Z, ThermoFisher) in PBS. Slides were incubated overnight at 4°C with a solution of primary antibodies: Mouse anti-human Pan Cytokeratin (1:100 diluted in blocking solution, Cat.# MCA1907, BioRad.), Mouse anti-human CD45 (1:100 diluted in blocking solution, Cat.# MCA87, BioRad), and Rabbit anti-human Vimentin (1:50 diluted in blocking solution, Cat.# 5741, Cell Signaling). After overnight incubation, slides were washed 3 times for 5 minutes each with PBS before incubating at room temperature for 1.5 hours with a solution of secondary antibodies: Goat anti-mouse Alexa Fluoro 546 (1:100 diluted in blocking solution, Cat.# A-21123, ThermoFisher), Goat anti-mouse Alexa Fluoro 488 (1:100 diluted in blocking solution, Cat.# A-21131, ThermoFisher), and Goat anti-rabbit Alexa Fluoro 647 (1:100 diluted in blocking solution, Cat.# A-21245, Thermo Fisher). After incubation slides were washed with PBS 3 times for 5 minutes each. Finally, a drop of ProLong Gold Mountant with DAPI (Cat. # P36935, ThermoFisher) was added to each slide followed immediately by a cover slip. Slides were imaged at 20x magnification using a Nikon Ti2 Eclipse. Each slide was individually assessed for CTC using the following criteria: Pan cytokeratin+/DAPI+/CD45-. Additionally, the expression level of vimentin was noted for each CTC.

Immunofluorescence staining for exosome study: For model sample experiments, pre-ultracentrifuged extracellular vesicles were stained using lipophilic dye, DiO. 1 µl of DiO staining dye (ThermoFisher, USA) was mixed with 100 µl of exosome solution and incubated for 20 minutes. After another ultracentrifugation to remove excess dye, the precipitated pellet was suspended with PBS and used for exosome capture experiments. For In-Vivo fluorescence imaging system, exosomes captured by the anti-CD63 bead were stained by immunofluorescence staining. Without release of captured exosomes, the exosome immobilized bead was directly followed by immunofluorescence staining for evaluation of cancer-associated marker expression. In order to evaluate the epithelial/mesenchymal properties on captured exosome by beads, we stained the exosome-specific bead with E-cadherin and vimentin, which are expressed on epithelial and mesenchymal exosomes, respectively. Because this marker usually expressed on

surface, we leaved out the permeabilization step. After fixation, exosome immobilized beads were labeled with staining dye containing Alexa fluor® 488-conjugated E-cadherin and PE-conjugated anti-human vimentin for 1 hour. After washing out excess dyes three times with PBS, the labeled beads were verified using In-Vivo imaging system.

Fluorescence verification using an in vivo imaging system: Spectral fluorescence images were obtained using Xenogen In-Vivo Imaging System (PerkinElmer, Waltham, MA). In order to obtain whole-body fluorescence images of the beads via non-destructive way, we utilized the equipment, which had been developed for in-vivo imaging of animal models. The FITC, TRITC, and Cy5 were detected at the wavelengths of 395 nm/509 nm, 554 nm/586 nm, 678 nm/694 nm (excitation/emission), respectively. Fluorescence images were gathered during 3~5 seconds of exposure time ($f/\text{stop} = 2$), and bright-field photographs were also obtained for each imaging time. Those images were merged and analyzed using Living Image 4.52 software (Caliper Life Sciences).

Protein extraction and western blot analysis for exosome: Exosome lysis was performed using RIPA buffer (Cat #: 89900, ThermoFisher Scientific, USA) with 1% protease inhibitor (Cat#: 78441, ThermoFisher Scientific, USA). The prepared buffer solution was applied to Exosome beads after exosome isolation and washing steps. Beads were incubated with RIPA buffer for 10 minutes in a conical tube and followed by mild centrifugation to collect supernatant. Total protein was measured by standard BCA analysis according to the manufacturer's instructions. Western Blot analysis was performed on a precast Stain Free 4–20% SDS gel from BioRad (Cat#: 4568094). The samples were prepared in 4x Laemelli buffer (Cat #: 161-0747, Bio-rad) with 2-mercaptoethanol and heated to 95°C for 5 minutes before loading onto the gel. The gel was run at 250 V for 28 minutes before transferring for 7 minutes onto an Immune-Blot low fluorescence PVDF membrane (Cat#: 1620261) using BioRad's TransBlot Turbo on their preset mixed molecular weight setting. Blocking was performed in 5% non-fat milk in TBST for 90 minutes. Primary antibodies were incubated overnight on a rocker at 4°C at a concentration of 1:500 (Flotillin-1, Santa Cruz, USA), 1:1000 (CD9, Cell Signaling; Calnexin, Cell Signaling, USA), or 1:1500 (Beta-Actin, Cell Signaling, USA) in 5% BSA milk in TBST. Thorough rinsing was performed, and then secondary antibody was incubated for 2 hours at room temperature (anti-Mouse, Santa Cruz; anti-Rabbit HRP, Cell Signaling, USA) at 1:1500 in 5% BSA milk in TBST.

Protein expression quantification from western blots: Following gel transfer using BioRad's TransBlot Turbo, the membrane was imaged using a ChemiDoc system (BioRad, USA) on their preset StainFree Blot setting. This image captured the total protein per lane. The membrane was then incubated with primaries, secondaries, and chemiluminescence before imaging using the same ChemiDoc system for the band of interest. Using BioRad's software, the total protein in each lane from the StainFree Blot image is compared to an arbitrary lane (usually the first lane with protein) to set a normalization factor for each subsequent lane. Moving to the image with the protein bands, each band is selected, the density is calculated, and the normalization is applied to calculate a normalized protein intensity for the band of interest. This number can then be compared between lanes.

Nanoparticle tracking analysis for circulating exosomes: For the profile analysis of isolated exosome and measurement of exosome concentration, nanoparticle tracking analysis (NTA) was performed using NanoSight NS300 (Malvern Instruments, UK). Sample of interest was loaded into the main instrument housing and the movement was monitored through a video sequence for 20 sec-

onds in duplicate. Data acquisition and processing were performed using NanoSight NS300 Control Software.

Acknowledgements

The authors thank Dr. Mina Zeinali for the assistance with Labyrinth experiments that are used as a label-free circulating tumor cell isolation technology. The authors acknowledge the Lurie Nanofabrication Facility at the University of Michigan. The authors acknowledge the financial support of the University of Michigan College of Engineering and NSF grant #DMR-0320740, and technical support from the Michigan Center for Materials Characterization. This work was supported by grants from National Institute of Health (NIH), 5-R33-CA-202867-02 to S.N. and 1-R01-CA-208335-01-A1 to S.N.

Conflict of Interest

S.N. is one of the named inventors on a patent for Microfluidic Labyrinth Technology granted to the University of Michigan. S.N. is also the co-founder of Labyrinth Biotech Inc. The funders and the company had no role in the design of the study; in the collection, analyses, or interpretation of data; in the writing of the manuscript; or in the decision to publish the results.

Keywords: antibodies · circulating tumor cells · exosomes · hydrogels · liquid biopsy

- [1] M. R. Speicher, K. Pantel, *Nat. Biotechnol.* **2014**, *32*, 441–443.
- [2] E. Heitzer, P. Ulz, J. B. Geigl, *Clin. Chem.* **2015**, *61*, 112–123.
- [3] N. Karachaliou, C. Mayo-de-las-Casas, M. A. Molina-Vila, R. Rosell, *Ann. Transl. Med.* **2015**, *3*, 36.
- [4] G. Sozzi, D. Conte, M. Leon, R. Cirincione, L. Roz, C. Ratcliffe, E. Roz, N. Cirenei, M. Bellomi, G. Pelosi, M. A. Pierotti, U. Pastorino, *J. Clin. Oncol.* **2003**, *21*, 3902–3908.
- [5] D. Madhavan, M. Wallwiener, K. Bents, M. Zucknick, J. Nees, S. Schott, K. Cuk, S. Riethdorf, A. Trumpp, K. Pantel, C. Sohn, A. Schneeweiss, H. Surowy, B. Burwinkel, *Breast Cancer Res. Treat.* **2014**, *146*, 163–174.
- [6] D. J. McBride, A. K. Orpana, C. Sotiriou, H. Joensuu, P. J. Stephens, L. J. Mudie, E. Hämäläinen, L. A. Stebbings, L. C. Andersson, A. M. Flanagan, V. Durbecq, M. Ignatiadis, O. Kallioniemi, C. A. Heckman, K. Alitalo, H. Edgren, P. A. Futreal, M. R. Stratton, P. J. Campbell, *Genes Chromosomes Cancer* **2010**, *49*, 1062–1069.
- [7] K. C. A. Chan, P. Jiang, Y. W. L. Zheng, G. J. W. Liao, H. Sun, J. Wong, S. S. N. Siu, W. C. Chan, S. L. Chan, A. T. C. Chan, P. B. S. Lai, R. W. K. Chiu, Y. M. D. Lo, *Clin. Chem.* **2013**, *59*, 211–224.
- [8] T. Lecomte, A. Berger, F. Zinzindohoué, S. Micard, B. Landi, H. Blons, P. Beaune, P. Cugnenc, P. Laurent-puig, *Int. J. Cancer* **2002**, *100*, 542–548.
- [9] J. A. Shaw, K. Page, K. Blighe, N. Hava, D. Guttery, B. Ward, J. Brown, C. Ruangpratheep, J. Stebbing, R. Payne, C. Palmieri, S. Cleator, R. A. Walker, R. C. Coombes, *Genome Res.* **2012**, *22*, 220–231.
- [10] A. R. Thiery, F. Moulire, S. El Messaoudi, C. Mollevi, E. Lopez-Crapez, F. Rolet, B. Gillet, C. Gongora, P. Dechelotte, B. Robert, M. Del Rio, P.-J. Lamy, F. Bibeau, M. Nouaille, V. Lorient, A.-S. Jarrousse, F. Molina, M. Mathonnet, D. Pezet, M. Ychou, *Nat. Med.* **2014**, *20*, 430–435.
- [11] E. Valtorta, S. Misale, A. Sartore-Bianchi, I. D. Nagtegaal, F. Paraf, C. Lauricella, V. Dimartino, S. Hobor, B. Jacobs, C. Ercolani, S. Lamba, E. Scala, S. Veronese, P. Laurent-Puig, S. Siena, S. Tejpar, M. Mottolose, C. J. A. Punt, M. Gambacorta, A. Bardelli, F. Di Nicolantonio, *Int. J. Cancer* **2013**, *133*, 1259–1265.
- [12] A. L. Isola, S. Chen, *Curr. Neuropharmacol.* **2017**, *15*, 157–165.
- [13] K.-L. G. Spindler, N. Pallisgaard, I. Vogelius, A. Jakobsen, *Clin. Cancer Res.* **2012**, *18*, 1177–1185.
- [14] D. Buschmann, A. Haberberger, B. Kirchner, M. Spornraft, I. Riedmaier, G. Schelling, M. W. Pfaffl, *Nucl. Acids Res.* **2016**, *44*, 5995–6018.
- [15] E. Crowley, F. Di Nicolantonio, F. Loupakis, A. Bardelli, *Nat. Rev. Clin. Oncol.* **2013**, *10*, 472–484.
- [16] B. Gold, M. Cankovic, L. V. Furtado, F. Meier, C. D. Gocke, *J. Mol. Diagn.* **2015**, *17*, 209–224.
- [17] C. Alix-Panabières, K. Pantel, *Ann. Transl. Med.* **2013**, *1*, 18.
- [18] J. B. Smerage, W. E. Barlow, G. N. Hortobagyi, E. P. Winer, B. Leyland-Jones, G. Srkalovic, S. Tejwani, A. F. Schott, M. A. O'Rourke, D. L. Lew, G. V. Doyle, J. R. Gralow, R. B. Livingston, D. F. Hayes, *J. Clin. Oncol.* **2014**, *32*, 3483–3489.
- [19] A. Goldkorn, B. Ely, D. I. Quinn, C. M. Tangen, L. M. Fink, T. Xu, P. Twardowski, P. J. Van Veldhuizen, N. Agarwal, M. A. Carducci, J. P. Monk, R. H. Datar, M. Garzotto, P. C. Mack, P. Lara, C. S. Higano, M. Hussain, I. M. Thompson, R. J. Cote, N. J. Vogelzang, *J. Clin. Oncol.* **2014**, *32*, 1136–1142.
- [20] M. Cristofanilli, T. Budd, M. J. Ellis, A. Stopeck, J. Matera, M. C. Miller, J. M. Reuben, G. V. Doyle, W. J. Allard, L. W. M. Testappen, D. F. Hayes, *N. Engl. J. Med.* **2004**, *351*, 781–791.
- [21] W. J. Allard, J. Matera, M. C. Miller, M. Repollet, M. C. Connelly, C. Rao, A. G. J. Tibbe, J. W. Uhr, L. W. M. M. Terstappen, *Clin. Cancer Res.* **2004**, *10*, 6897–6904.
- [22] S. Nagrath, L. V. Sequist, S. Maheswaran, D. W. Bell, D. Irimia, L. Ulkus, M. R. Smith, E. L. Kwak, S. Digumarthy, A. Muzikansky, P. Ryan, U. J. Balis, R. G. Tompkins, D. A. Haber, M. Toner, *Nature* **2007**, *450*, 1235–1239.
- [23] C. Alix-Panabières, K. Pantel, *Clin. Chem.* **2013**, *59*, 110–118.
- [24] C. Alix-Panabières, K. Pantel, *Cancer Dis.* **2012**, *2*, 974–975.
- [25] A. Bardia, D. A. Haber, *J. Clin. Oncol.* **2014**, *31*, 3470–3471.
- [26] S. Wang, H. Wang, J. Jiao, K.-J. Chen, G. E. Owens, K.-I. Kamei, J. Sun, D. J. Sherman, C. P. Behrenbruch, H. Wu, H.-R. Tseng, *Angew. Chem. Int. Ed. Engl.* **2009**, *48*, 8970–8973.
- [27] S. L. Stott, C. H. Hsu, D. I. Tsukrov, M. Yu, D. T. Miyamoto, B. A. Waltman, S. M. Rothenberg, A. M. Shah, M. E. Smas, G. K. Korir, F. P. Floyd Jr, A. J. Gilman, J. B. Lord, D. Winokur, S. Springer, D. Irimia, S. Nagrath, L. V. Sequist, R. J. Lee, K. J. Isselbacher, S. Maheswaran, D. A. Haber, M. Toner, *Proc. Nat. Acad. Sci.* **2010**, *107*, 18392–18397.
- [28] D. A. Bichara, X. Zhao, N. S. Hwang, H. Bodugoz-Senturk, M. J. Yaremchuk, M. A. Randolph, O. K. Muratoglu, *J. Surg. Res.* **2010**, *163*, 331–336.
- [29] M. Bahadoran, A. Shamloo, Y. D. Nokoorian, *Sci. Rep.* **2020**, *10*, 7342.
- [30] G. Wu, K. Jin, L. Liu, H. Zhang, *Soft Matter* **2020**, *16*, 3319–3324.
- [31] S. T. Bendtsen, S. P. Quinnell, M. Wei, *J. Biomed. Mater. Res.* **2017**, *105*, 1457–1468.
- [32] Y.-T. Kang, T. Hadlock, T.-W. Lo, E. Purcell, A. Mutukuri, S. Fouladdel, M. D. S. Raguera, H. Fairbairn, V. Murlidhar, A. Durham, S. A. McLean, S. Nagrath, *Adv. Sci.* **2020**, *7*, 2001581.
- [33] N. A. Peppas, J. Z. Hilt, A. Khademhosseini, R. Langer, *Adv. Mater.* **2006**, *18*, 1345–1360.
- [34] M. W. Tibbitt, K. S. Anseth, *Biotechnol. Bioeng.* **2009**, *103*, 655–663.
- [35] R. Mahou, R. P. H. Meier, L. H. Bühler, C. Wandrey, *Materials* **2014**, *7*, 275–286.
- [36] K. Y. Lee, D. J. Mooney, *Chem. Rev.* **2001**, *101*, 1869–1879.
- [37] Z. Fan, B. Liu, J. Wang, S. Zhang, Q. Lin, P. Gong, L. Ma, S. Yang, *Adv. Funct. Mater.* **2014**, *24*, 3933–3943.
- [38] Y. Qiu, K. Park, *Adv. Drug Delivery Rev.* **2001**, *53*, 321–339.
- [39] G. Fuhrmann, R. Chandrawati, P. A. Parmar, T. J. Keane, S. A. Maynard, S. Bertazzo, M. M. Stevens, *Adv. Mater.* **2018**, *30*, 1706616.
- [40] Y.-T. Kang, Y. J. Kim, T. H. Lee, Y.-H. Cho, H. J. Chang, H.-M. Lee, *Sci. Rep.* **2018**, *8*, 15218.
- [41] E. Choi, Y. Choi, Y. H. P. Nejad, K. Shin, J. Park, *Sens. Actuators B* **2013**, *180*, 107–113.
- [42] T. B. Tran, S. Cho, J. Min, *Biosens. Bioelectron.* **2013**, *50*, 453–459.
- [43] N. Golafshan, R. Rezaehani, M. T. Esfahani, M. Kharazilha, S. N. Khorasani, *Carbohydr. Polym.* **2017**, *176*, 392–401.
- [44] L. L. Palmese, R. K. Thapa, M. O. Sullivan, K. L. Kiick, *Curr. Opin. Chem. Eng.* **2019**, *24*, 143–157.
- [45] M. D. Miljkovic, F. A. Flomerfelt, R. E. Gress, Abstract 313, AACR Annual Meeting 2017; April 1–5, 2017; Washington, DC.
- [46] Y.-J. Chiu, W. Cai, Y. V. Shih, I. Lian, Y.-H. Lo, *Small* **2016**, *12*, 3658–3666.
- [47] A. Lecharpentier, P. Vielh, P. Perez-Moreno, D. Plancharde, J. C. Soria, F. Farace, *Br. J. Cancer* **2011**, *105*, 1338–1341.
- [48] C. R. Lindsay, V. Faugeroux, S. Michiels, E. Pailler, F. Facchinetti, D. Ou, et al. *Ann. Oncol.* **2017**, *28*, 1523–1531.

- [49] E. Lin, L. Rivera-Báez, S. Fouladdel, H. J. Yoon, S. Guthrie, J. Weiger, Y. Deol, E. Keller, V. Sahai, D. M. Simeone, M. L. Burness, E. Azizi, M. S. Wicha, S. Nagrath, *Cell Syst.* **2017**, *5*, 295–304.
- [50] M. Zeinali, M. Lee, A. Nadhan, A. Mathur, C. Hedman, E. Lin, R. Harouaka, M. S. Wicha, L. Zhao, N. Palanisamy, M. Hafner, R. Reddy, G. P. Kalemkerian, B. J. Schneider, K. A. Hassan, N. Ramnath, S. Nagrath, *Cancers* **2020**, *12*, 127.
- [51] Y. Wang, Y. Liu, L. Zhang, L. Tong, Y. Gao, F. Hu, P. P. Lin, B. Li, T. Zhang, *J. Cancer Res. Clin. Oncol.* **2019**, *145*, 2911–2920.
- [52] S. S. Tan, Y. Yin, T. Lee, R. C. Lai, R. W. Yeo, B. Zhang, A. Choo, S. K. Lim, *J. Extracell. Vesicles* **2013**, *2*, 22614.
- [53] A. J. Armstrong, M. S. Marengo, S. Oltean, G. Kemeny, R. L. Bitting, J. D. Turnbull, C. I. Herold, P. K. Marcom, D. J. George, M. A. Garcia-Blanco, *Mol. Cancer Res.* **2011**, *9*, 997–1007.
- [54] W. Lee, B.-K. Oh, Y. M. Bae, S.-H. Paek, W. H. Lee, J.-W. Choi, *Biosens. Bioelectron.* **2003**, *19*, 185–192.
- [55] J. Bu, Y.-T. Kang, Y. J. Kim, Y. H. Cho, H. J. Chang, H. Kim, B. I. Moon, H. G. Kim, *Lab Chip* **2016**, *16*, 4759–4769.
- [56] Y.-T. Kang, Y. J. Kim, J. Bu, Y. H. Cho, S. W. Han, B. I. Moon, *Nanoscale* **2017**, *9*, 13495–13505.

Manuscript received: May 21, 2021
Revised manuscript received: June 3, 2021
Accepted manuscript online: June 4, 2021
Version of record online: June 22, 2021